Wave Drag and Wave Patterns by Ships Moving in a Single-File Formation

Fengshen Zhu (朱风绅), Zhiming Yuan[1] (元志明)
Department of Naval Architecture, Ocean & Marine Engineering, University of Strathclyde, Glasgow, G4 0LZ, UK

Abstract: To minimize energy expenditure for each individual, animals adopt distinctive formations, such as fish schooling, 'V' formation by flying birds, and single-file formation by waterfowls. The phenomenon of ducklings following their mothers in a single-file configuration has been revealed by the mechanism of wave-riding and wave-passing. Drawing inspiration from this phenomenon, an investigation is undertaken on ships moving in a single-file formation. The objective is to quantify how much energy can be saved in different configurations. In this study, a three-dimensional boundary element method incorporating linear free surface boundary conditions is used to obtain the wave drag and wave patterns. It is found that when the constructive wave interference occurs in a two-ship formation, the wave resistance of the trailing ship increases and the leading ship experiences a decrease in its wave drags, especially when the two ships are in close proximity. Mutual benefit arises when destructive wave interference occurs between two ships. In addition, increasing the size of the trailing vessel facilitates the effect of wave-riding by leading ship, but this effect becomes less pronounced as the speed increases. In a multi-ship formation configuration, changing the size of the leading ship will have a localized effect on the wave-passing, but the fleet will eventually tend to a dynamic equilibrium. When the position of the first trailing vessel is changed, there is similarly a localized effect on the wave-passing. Adjusting the first trailing ship to the position of the constructive wave interference is not favorable to reduce its own drag but enhances the wave-riding effect of its close follower. Finally, to achieve the wave-passing, the trailing ship does not necessarily have to occupy an optimum position. This can still be accomplished if the trailing ship moves backward by an integer multiple of wavelength.

Keywords: wave-riding; wave-passing; single-file ship formation; wave drag; wave patterns.

1 Introduction

Animals in nature often migrate in distinctive formations, which can reduce energy expenditure and enhance their locomotion performance. Schooling fish increases

[1] Corresponding author email: zhiming.yuan@strath.ac.uk

their migratory endurance by adjusting their swimming posture and effectively harnessing the energy from environmental vortices generated by neighboring individuals[1-4]. Birds fly in a 'V' formation to minimize individual effort by utilizing the upwash of the vortex region behind their fellow companion's wingtips[5-11]. Ducklings swimming in a single-file formation can significantly reduce their metabolic exertion by efficiently transferring momentum from the mother duckling to the smaller ones through the generation and utilization of vorticity[12, 13]. However, a new insight provided by Yuan et al.[14] to shed light on this bioimprinting behavior, attributing it to wave-riding and wave-passing. The first duckling effectively rides on the waves created by its mother, transferring these waves to its siblings. The subsequent ducklings can move forward without any effort, by positioning themselves optimally. The wave energy, initiated by the mother duck, passes through the entire formation, from the first to the last duckling, finally dispersing in the form of Kelvin wave pattern. Drawing inspiration, Yuan[15] and Ellingsen[16] highlighted that waterborne traffic can similarly harness these hydrodynamic benefits.

To minimize the total wave drag, multi-hull vessels are expertly engineered by harnessing the cancellation effects between waves generated by the hulls. Wilson et al.[17] conducted both analytical predictions and towing basin validation experiments for the Wave Cancellation Multihull (WCM) of a trimaran at the David Taylor Model Basin. Based on the thin ship theory, Tuck[18] systematically studied a family of multihull ships by varying the number of hulls, their placement, and beams, while maintaining the total displacement of the vessel as well as the individual length and shape of each hull constant. The optimum configurations for two, three, and four-hulled vessels are determined, considering both configurations with and without longitudinal stagger, across a broad spectrum of speeds. Similarly, Peng[19] investigated the effect of wave interference on the wave resistance of a family of multihull ships within the framework of thin ship theory. The study focused on the steady motion of ships on an unbounded free surface of deep water and the wave resistance and wave patterns are computed and analyzed by varying relative positions of the hulls. Yu et al.[20] explored the prospective optimal di-hull configurations by towing-tank tests and longitudinal wave-cut analysis. The resistance-reduction predicted by the thin ship theory was evaluated by comparing it with experimental results, and the usefulness and limits of the theory are examined. The CFD analyses have also been widely employed for conducting comprehensive studies on multihull ships. The wave interference effects between the outriggers and center-hull on the resistance of a trimaran are researched by Yildiz et al.[21], based on the turbulence model of unsteady Reynolds-averaged Navier-Stokes (URANS). Deng et al[22] explored the effects of trim and sinkage on the resistance performance of a trimaran under different scenarios. They performed numerical simulations of the free and captive models as well as the free model with T-foil and compared them with experiments. Nazemian and Ghadimi[23] studied the trimaran hull optimization by using a multi-objective optimization platform. The Arbitrary Shape Deformation (ASD) technique and Simcenter SHERPA algorithm were applied for geometry optimization.

In recent years, various ship formations have been increasingly explored to enhance fuel efficiency in maritime operations. A leader-follower ship fleet was studied by Ma et al.[24], via a 4-point model and Neumann-Michell potential computation. They derived the destructive wave interference region for the follower under different speeds and found the destructive interference was invalid at low or high Froude numbers. Liu et al.[25] explored the wave resistance and flow field of two KRISO Container Ships (KCS) moving in a line at various speeds and intervals, utilizing the Reynolds-Averaged Navier-Stokes (RANS) method. They attributed the reduction in wave drag for the trailing ship to the superposition of waves around the following vessel with the transverse waves created behind the leading ship. He et al.[26] adopted the Shear Stress Transport (SST) k–ω turbulence model to analyze three distinctive ship formations. They found that tandem formation was the most energy efficient, followed by triangular and parallel formation. Dong et al. studied the echelon formation of unmanned surface vehicles (USVs), analyzing how different spacing configurations influence their friction and pressure resistances[27]. They categorized the aft wedge region into five zones, distinguishing them by calculating the positive and negative attributes of the energy consumption index. They also developed a dynamic formation optimization strategy to construct an energy-saving formation[28]. The swarm intelligence algorithm was integrated into the framework of robust optimization over time (ROOT) to determine the optimal position layout. In addition, Lambert and Brizzolara[29] adopted a high-order free-surface Rankine source boundary element method and Qin et al.[30] employed STAR-CCM+ to investigate the hydrodynamic interference in multi-ship formations with varying longitudinal and lateral offsets.

The US Defense Advanced Research Projects Agency has proposed the Sea Train[31] concept in 2020, closely akin to ducklings in a single file formation. As illustrated in Figure 1, it envisages a formation of four or more unmanned surface vehicles aligned in a row to minimize collective wave-making resistance, effectively creating 'the equivalent of a long parallel mid-body'. Compared to a vessel with an extended parallel mid-body, the formation of multiple shorter ships in single file can offer numerous advantages, such as enhanced mobility, maneuverability, and flexibility. The research of Yuan et al.[14] and Yuan[15] indicated that the wave patterns behind ships/ducklings can be replicated by their followers as long as they maintain an optimal position and maintain uniform separation, termed wave-passing. However, this phenomenon arises some intriguing questions:

- Does the wave-passing phenomenon persist if any trailing ships are not in an optimum position?
- Can trailing ships extract more wave energy by increasing the size of the leading ship?
- Can the leading ship extract more wave energy by increasing the size of the trailing ship?
- Will the drag reduction effect of the other ships get better or worse if the position of one trailing ship in the formation changes?

In this paper, we revisit different movement formations of animals in nature and further review the hydrodynamic interference by multihull ships and ship formations of various configurations in naval architecture. To investigate the steady wave interference by ships moving in a single-file formation on calm water, a boundary element method with linear free surface boundary condition is adopted. The effects of spacing between two ships and the size of the trailing ship on the wave drag reduction are analyzed when one ship follows another. In a formation comprising more than one trailing ship, the phenomenon of wave-passing is further explored, by considering the size of the leading ship, the position of the initial trailing ship, and the optimal positions for each trailing ship.

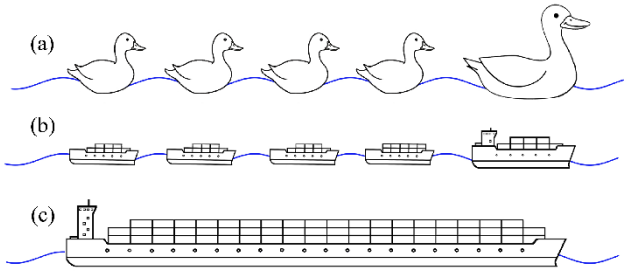

Figure 1. (a) Four ducklings following their mother in a single-file formation. (b) Four trailing ships following the leading ship in a single-file formation. (c) A ship with a very long parallel mid-body.

2 Methodology and Assumptions

The resistance experienced by a ship in steady motion on calm water is typically composed of skin friction resistance, wave-making resistance, eddy-making resistance, and wind and air resistance[32]. The present study mainly focuses on the wave-making resistance, without delving into the analysis of other components of ship resistance. To quantify the wave drag of ships moving in single-file formation, the following assumptions are made.

(1) The frictional resistance is primarily influenced by the water's viscosity, the surface roughness of the body, and the wetted area. It is assumed that the difference in frictional resistance between sailing alone and sailing in a formation is negligible for vessels moving at the same speed.

(2) The presence of rudders, tail post and propeller shaft mounts lead to flow separation and ultimately to the formation of vortices and eddies. The additional drag induced by bilge vortices may also result in energy losses. However, with proper design, vortex drag can be avoided or reduced to negligible levels.

(3) The total resistance of the ship is significantly impacted by the prevailing sea state. Wind exerting force on the water's surface above the ship results in additional drag. However, owing to the relatively low density of wind,

this is generally minor compared to water resistance. Furthermore, the interaction between the ship and wave currents may also increase added resistance. In this study, it is assumed that the ship is sailing in calm waters and is therefore not affected by weather conditions.

(4) The issue of wave-making can be examined through two perspectives: force and motion. The focus here is on how a ship's resistance changes while in formation movement, excluding aspects related to trimming or sinkage.

(5) The effect of the ship on the water typically does not lead to a variation in the water's density, hence the assumption that the water is an incompressible fluid is applied.

Based on the above assumptions, it can be inferred that the resistance of a ship mainly originates from two aspects: friction and wave-making. Since the concern here is with the wave-making problem, friction due to viscosity is not considered. The fluid domain can be described by a velocity potential -φ satisfying the Laplace's equation:

$$\frac{\partial^2 \varphi}{\partial x^2} + \frac{\partial^2 \varphi}{\partial y^2} + \frac{\partial^2 \varphi}{\partial z^2} = 0. \tag{1}$$

A mathematical model has been established to investigate the wave-making problems of ships moving in single-file formation. The boundary element method (BEM) based on a three-dimensional potential flow theory can be used to calculate the wave drag of ships. It is worth noting that the leading ship and trailing ships are assumed to move with the same speed U and the same direction, so the vessel encountering or overtaking will not take place. For a formation of ships with the forwarding speed, two sets of right-handed coordinate systems are established with a global reference O-xyz fixed to the earth and a local reference O-$x_iy_iz_i$ (i=1,2,3…) fixed to each ship, as shown in Figure 2. The shallow water effect is not considered in the present numerical calculations and the velocity potential is time-independent in the body-fixed frame. Since the ship moving speed is constant, the hydrodynamic interaction can be handled by a steady state problem. By combining kinetic and dynamic free-surface conditions, it satisfies the time-independent linearized steady free surface condition:

$$U^2 \frac{\partial^2 \varphi}{\partial x^2} + g \frac{\partial \varphi}{\partial z} = 0, \tag{2}$$

where g is the gravitational acceleration. The boundary condition of the ship surface should meet that there is no flow through the body surface,

$$\frac{\partial \varphi}{\partial n} = Un, \tag{3}$$

where $n=(n_1,n_2,n_3)$ is the unit vector inward on the wetted body surface. In addition, a radiation condition is applied to the control surface to ensure that the wave disappears at infinity:

$$\varphi \to 0, \zeta \to 0, as \sqrt{x^2 + y^2} \to \infty, \tag{4}$$

where ζ is the wave elevation. An in-house numerical program MHydro is adopted to solve the boundary value problem (BVP) established by equation (1) to (4). This program has been extensively validated by multi-body hydrodynamic interaction tests with ship models, and the details of numerical implementation can be found in Yuan[33]. It should be particularly noted that one cannot consider the infinite free surface domain. To remove wave reflections and enhance numerical stability, the computational domain needs to be truncated at a suitable distance from the moving ship. Moreover, a second-order upwind discretization scheme is employed on the free surface to ensure that the waves can propagate to the far field.

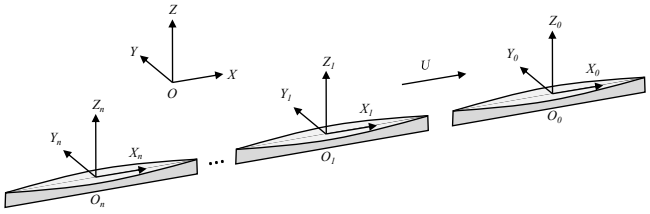

Figure 2. Coordinate systems.

Once the unknown potential φ is solved, the steady pressure over the wetted hull surface can be calculated from linearized Bernoulli's equation:

$$p = \rho U \frac{\partial \varphi}{\partial x}, \tag{5}$$

where ρ is the water density. Integrating the pressure on the wetted hull surface, the force (or moment) can be obtained by

$$F_i = \iint p n_i ds \;\; i = 1,2, \ldots ,6, \tag{6}$$

where i=1, 2, ..., 6, represent surge, sway, heave, roll, pitch and yaw, respectively.

The wave making resistance is equal to the component of the force in the surge direction. From the boundary conditions of the dynamic free surface, the wave elevation can be derived in the form,

$$\zeta = \frac{U}{g} \frac{\partial \varphi}{\partial x}. \tag{7}$$

The wave drag experienced by a ship moving individually is denoted as R_s and the wave drag of the n-th ship moving in a single-file formation is denoted as R_n. The drag reduction coefficient is defined by

$$C_{DR} = \left(1 - \frac{R_n}{R_s}\right) \times 100\%. \tag{8}$$

$C_{DR} > 0$ indicates the wave resistance is reduced in a formation due to the hydrodynamic interaction; whilst $C_{DR} < 0$ represents an increase in wave resistance. No interaction is found at $C_{DR} = 0$, and the wave resistance is the same as that of independent moving. Here, n denotes the number of ships in the formation, and $n = 0$ denotes the leading ship.

3 Wave-riding phenomenon

3.1 Numerical model and convergent test

A blunt Wigley hull[34] with $L/B = 5{:}1$ and $L/D = 10{:}1$ is adopted in the numerical calculation, where L, B and D are the ship length, breadth, and draft, respectively. The convergence study analyzes the wave drag reduction of the trailing ship when two identical ships move in a single-file formation with varying gaps. The gap between the stern of the leading ship and the bow of the trailing ship is denoted by G_{01}, as illustrated in Figure 4. The convergence of the mesh size on the free surface is verified by varying the element size in the x and y directions. Three mesh size schemes are selected, i.e., $L/dx \times B/dy = 30\times5$ (coarse mesh), 40×10 (intermediate mesh), 50×15 (fine mesh), where dx and dy denote the length and width of each mesh. In Figure 3(a), the differences between fine and medium meshes in the amplitude of the C_{DR} peak values are: $\Delta\mu_1/\mu_{11}$=7.3% and $\Delta\mu_2/\mu_{21}$=10.6%. In addition, the differences between fine and medium meshes in the wavelength of the C_{DR} peak values are: $\Delta\chi_1/\chi_{11}$=3.4% and $\Delta\chi_2/\chi_{21}$=3.4%. These discrepancies are attributed to the numerical dispersion and damping inherent in the Rankine source method[35]. For optimal computation accuracy and efficiency, a grid configuration of 40×10 is employed. Similarly, the mesh configuration of $L/dx\times D/dz = 40\times10$, where dz represents the mesh size in the z-direction, is applied to the body surface, with results compared in Figure 3(b).

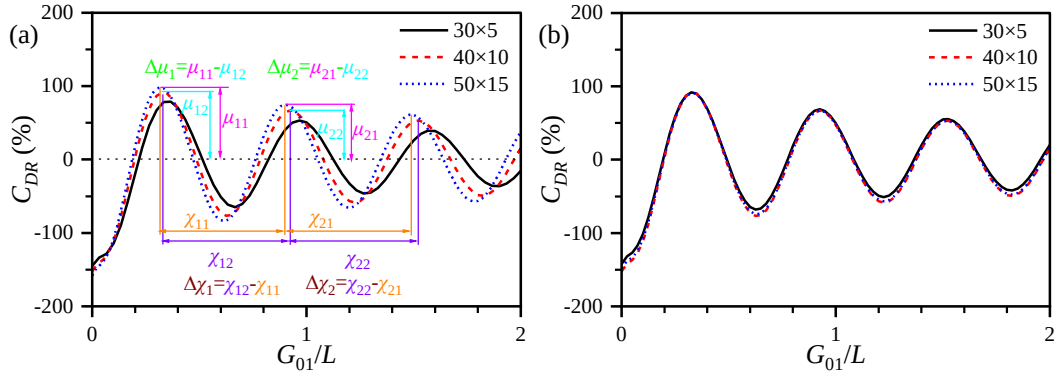

Figure 3. Convergence study of two identical ships moving at $F_r = 0.3$ in a single-file formation for (a) free surface and (b) body surface.

Figure 4 illustrates the panel distribution of the free surface and wetted body surface of two navigating ships in a single-file formation. To save computational resources,

only half of the computational domain is modelled. Additionally, to simulate the full Kelvin wave pattern and to avoid the wave reflection, the computational domain is extended to $1L$ upstream from the center of the leading ship, $3L$ downstream from the center of the trailing ship, and $8B$ sideways from the center of both ships.

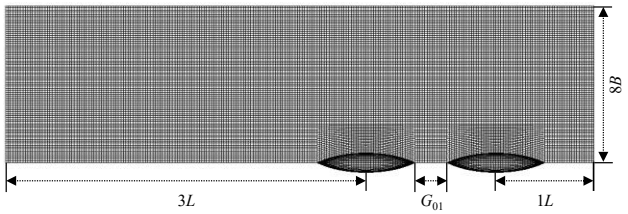

Figure 4. Computational domain and panel distribution of two ships moving in a single-file formation. There are 15440 panels distributed over the entire computational domain: 13840 panels on the free surface, 800 panels on the wetted surface of each ship.

3.2 Wave-riding by the trailing ship

A single-file ship formation including one leading ship and one trailing ship advancing at $F_r = 0.3$ is investigated. F_r is the Froude number, which can be expressed by

$$F_r = \frac{U}{\sqrt{gL}}. \tag{9}$$

The reduction in wave resistance for each ship can be obtained by placing the leading ship at the origin and by changing the position of the trailing ship from -$1L$ to -$4L$.

Figure 5(a) illustrates the variations in wave drag reduction for both the leading ship and the trailing ship across different spacings, along with the wave patterns along the centerline in the wake of the leading ship. Within the distance range of -$1L$ to -$4L$, the wave drag reduction of the trailing ship demonstrates a periodic oscillation around zero, with the oscillation amplitude decreasing as the distance between the vessels increases. This rate of attenuation is consistent with the diminishing wave patterns generated by the leading ship, which spread and decay as they travel downstream. Notably, when the vessels are in closer proximity, the leading ship benefits from a substantial reduction in wave drag. However, as the gap widens, the leading ship has a diminishing advantage in wave reduction resistance, a phenomenon attributable to the downstream radiation of the Kelvin wave pattern.

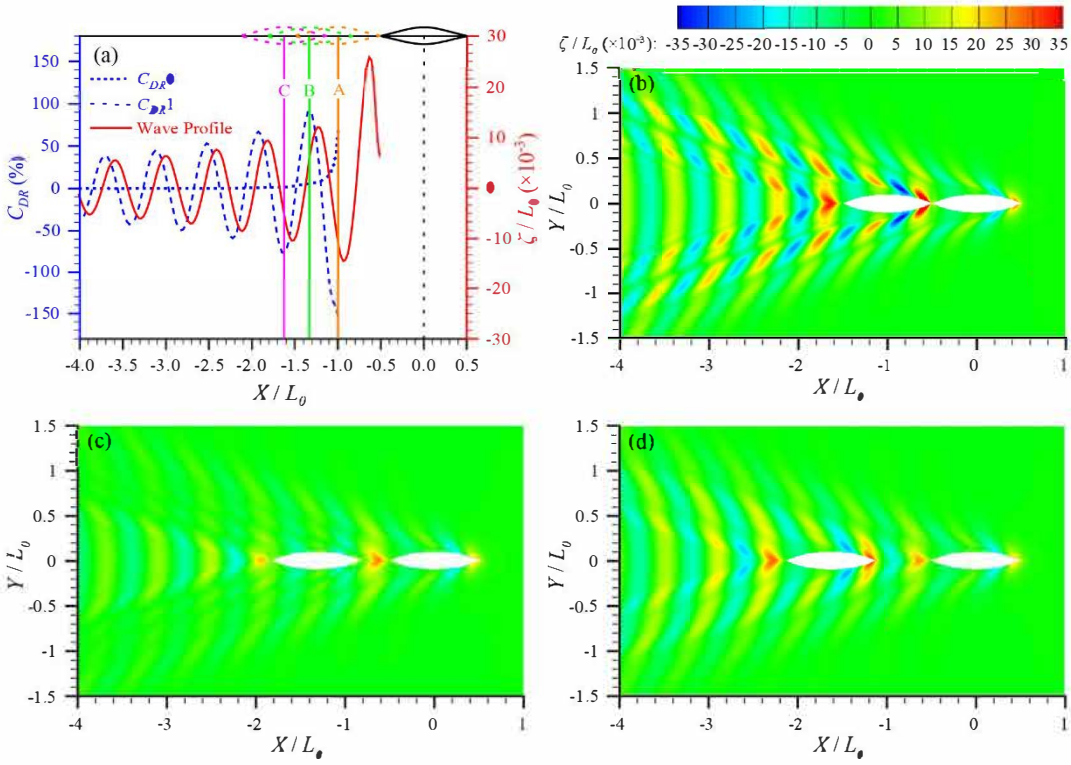

Figure5. (a) Wave drag reduction of the leading ship (n = 0, blue dot curve) and the trailing ship (n = 1, blue dash curve) with different distances at $F_r = 0.3$. Positions A, B and C represent the typical positions of wave interference. The wave profile on the center line behind the leading ship is denoted by the orange curve. (b) (c) (d) Wave patterns when the trailing ship is moving at position A, B, and C, respectively.

There are three distinct positions, labelled as A, B, and C, where various wave interference phenomena occur between the two ships. When the trailing ship (positioned at point A) closely follows the leading ship, the wave drag of the leading vessel is significantly reduced by 67%. On the other hand, the trailing ship experiences a negative wave drag reduction of -152%, which implies that it consumes 1.5 times more energy compared to when it navigates independently. As elucidated in Figure 5(b), a high-pressure distribution is observed at the stern of the leading ship and the bow of the trailing ship. This arises due to the superimposition of the rear wave generating from the leading ship and the frontal wave produced by the trailing ship. Such a condition proves beneficial for the leading ship in terms of energy conservation, but it is disadvantageous for the trailing ship, impeding its ability to reduce wave resistance.

When the trailing vessel occupies Position B, a win-win scenario arises. The wave drag on the trailing ship is drastically reduced by 91%, indicating that its total wave drag is a mere 9% of that experienced by a solitary ship moving at a similar speed. Simultaneously, the wave drag on the leading ship experiences a reduction of 6%. This reciprocal advantage is pivotal in establishing the optimal ship

formation, with an emphasis on minimizing the overall wave resistance. Figure 5(c) shows the wave pattern when the trailing ship is at position B. The bow of the trailing vessel is precisely positioned at the wave trough, resulting in the cancellation of the bow wave. Conversely, the stern of the trailing vessel is situated exactly at the wave crest, leading to constructive wave interference. The combination of wave cancellation at the bow and wave construction at the stern induces a propulsion force in the vessel, which can effectively overcome the wave resistance.

When the trailing vessel reaches position C, the wave drag experienced by this ship increases by 76%. This phenomenon is depicted in Figure 5(d). The phase of the wave generated by the trailing vessel precisely synchronizes with that of the leading ship, resulting in the amplification of the wave amplitude through wave superposition. Consequently, the bow of the trailing ship is positioned atop the crest, whilst its stern resides in the trough. This leads to an unexpected added resistance of the ship, which is detrimental to reduce wave drag.

3.3 Wave-riding by the leading ship

Various configurations of ships, comprising a leading vessel and a trailing vessel of differing dimensions, are explored. The dimensions of the leading ship remain constant, whilst the size of the trailing ship is proportionally scaled, involving simultaneous alterations in length, breadth, and draught. Here, the scale of the trailing ship relative to the leading ship is indicated by L_1/L_0. As elucidated in Section 3.2, when the trailing ship occupies position A, the leading ship may derive maximal advantage, albeit at the expense of the trailing ship. Conversely, at position B, both the leading and trailing ships may attain mutual benefits. Specifically, the leading ship receives the greatest wave drag reduction when the trailing ship is at position A, while the trailing ship experiences its peak C_{DR} at position B. Consequently, positions A and B are selected for the investigation of the dimensions of the trailing ship on the wave resistance of the leading ship, under varying travel speeds. It should be noted that position B is variable, contingent upon the differing velocities.

The wavelength λ on the centerline behind the leading ship is related to the velocity U, which can be expressed by

$$\lambda = \frac{2\pi U^2}{g}. \tag{10}$$

Hence, the wavelength has been selected as the primary criterion, given that the intricate interplay between the length of a vessel and its corresponding wavelength is crucial in determining the wave interference observed between two ships.

Figure 6(a) and (b) depict the variation in wave resistance of the leading ship as the size of the trailing ship increases from 0.5 to 2.5, positioned respectively at locations A and B. The wavelengths generated by the leading or trailing ship at

various velocities are quantified without dimension, in relation to the length of the leading ship, with a range incrementing from 0.25 to 2. The non-dimensional speed (F_r) corresponding to the wavelengths are labelled on the top axis. Owing to the constraints in numerical calculation mesh size, the optimal position B is not ascertained with absolute precision. Consequently, an error bar is incorporated in Figure 6(b). Conversely, the inclusion of an error bar in Figure 6(a) is deemed unnecessary, given the absence of any gap between the two vessels at Position A. The error bar is defined by

$$Error = \sqrt{\frac{\sum_{i=1}^{m}\left(C_{DR_i} - \overline{C_{DR}}\right)^2}{m-1}}. \tag{11}$$

The C_{DR} values for each ship are calculated by considering three consecutive mesh positions to ensure that the accurate position falls within these intervals. Thus, m=3 is used in the error bar calculation and $\overline{C_{DR}}$ represents the mean value of these three C_{DR} values.

At both positions, as the size ratio L_1/L_0 increases, the wave drag reduction tends to increase, especially noticeable for lower travelling speeds. However, there is a large difference in the scale of wave drag reduction between the two positions. Position A exhibits a much higher percentage change in wave drag reduction across all size ratios and speeds compared to Position B. Upon examination of Figure 7(a), it becomes apparent that the wave energy present at Position A is considerably greater than that at Position B, particularly within the high-pressure region at the stern of the leading vessel.

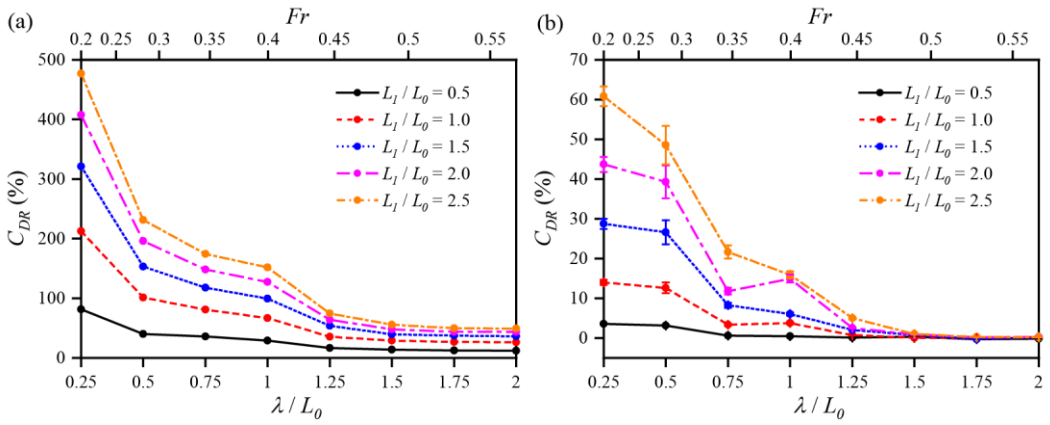

Figure6. (a) (b) Effect of the size of the trailing ship on the drag of the leading ship when trailing ship is at Position A and B, respectively.

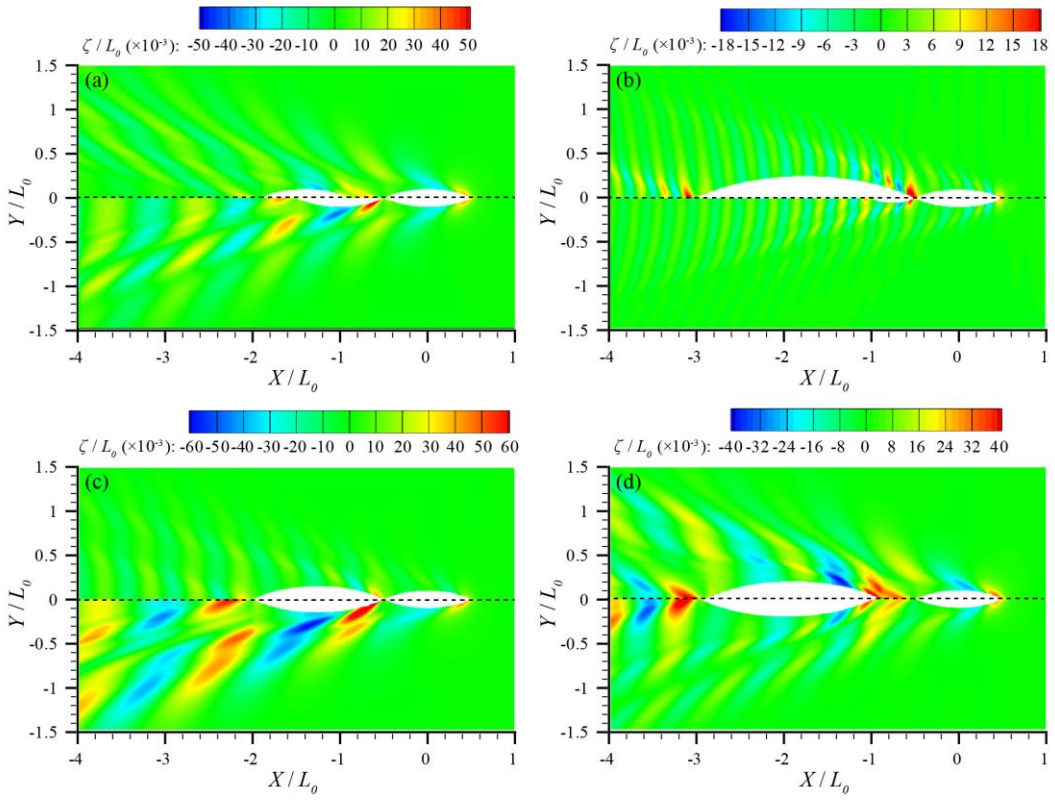

Figure7. (a)Wave patterns of position A (lower) and B (upper) at $\lambda/L_0 = 1$. (b) Wave patterns of $L_1/L_0 = 2.5$ (upper) and 0.5 (lower) at $\lambda/L_0 = 0.25$. (c) Wave patterns of $\lambda/L_0 = 0.5$ (upper) and 1.5 (lower) with $L_1/L_0 = 1.5$. (d) Wave patterns of $\lambda/L_0 = 1$ (upper) and 0.75 (lower) with $L_1/L_0 = 2$.

The C_{DR} for the leading vessel is approximately 480% in the scenario where the size ratio is 2.5 at Position A when $\lambda/L_0 = 0.25$. This indicates that the leading vessel does not require any energy expenditure for its propulsion; rather, it is effectively propelled forward by the frontal waves created by the trailing ship. Conversely, when the size ratio is 0.5, the propulsion force transmitted from the trailing ship is capable to offset approximately 80% of the wave drag experienced by the leading ship. As shown in Figure 7(b), the high-pressure zone at the stern of the leading ship is more expansive and the energy density significantly greater for a size ratio of 2.5 than for a size ratio of 0.5.

Moreover, as the moving speed increases, there is a substantial decline in the wave drag reduction across each size ratio. Concurrently, the differences in C_{DR} between different size ratios diminish, and the curves tend to converge. Figure 7(c) offers a comparative visualization of the wave patterns of $\lambda/L_0 = 0.5$ and 1.5 with $L_1/L_0 = 1.5$. The convergence of the C_{DR} is highly relevant to how we define C_{DR} in Eq. (8). At lower speed (λ/L_0 is small), the denominator in Eq. (8) is small. A fluctuation of the numerator, which is highly relevant to the hydrodynamic interaction, could

result in a very large C_{DR}. As the speed increases, the wave resistance of the trailing and leading ship both increases dramatically. The interaction also becomes more intense. The ratio Rn and Rs turns to be convergent, indicating higher speeds will result in more intense hydrodynamic interactions.

Nevertheless, it is observed that some C_{DR} values at lower travelling speeds do not surpass those at higher speeds when at Position B. For instance, the C_{DR} observed at $\lambda/L_0 = 1$ exceeds that at $\lambda/L_0 = 0.75$ for both L_1/L_0 ratios of 2 and 1. This is because the gap between two ship for $\lambda/L_0 = 0.75$ is larger than that for $\lambda/L_0 = 1$, which is detrimental to the formation of a high-pressure zone at the stern of the leading ship, owing to the reduced wave superposition. Figure 7(d) illustrates the wave patterns for $\lambda/L_0 = 1$ and 0.75, with a size ratio $L_1/L_0 = 2$, while the trailing ship is at Position B. At $\lambda/L_0 = 1$, the trailing ship is perfectly positioned to ride atop two waves. In contrast, for λ/L_0= 0.75, the trailing ship is required to move back to take advantage of the wave-riding

4 Wave-passing phenomenon

The research results[14, 15] show how the waves generated by the leading ship are passed to the trailers by maintaining uniform distance between each other. Here, the phenomenon of the wave-passing is further explored by changing the ship formation configurations.

4.1 Passing the waves from different leading ships

In designing ship formations, the size of the leading ship is intuitively a significant factor that influences how much drag reduction can be achieved by the trailing ship. Consequently, in varying ship formations, the leading ship's size is altered while the dimensions of the trailing vessels are maintained constant. The scale of the leading ship relative to the trailing ship is denoted by the ratio L_0/L_1. Since the size of the leading ship is variable, the moving speed is nondimensionalized by the trailing ship's size, with $F_r = 0.3$. The wave drag reduction coefficient C_{DR} of the leading ship and its trailers is shown in Figure 8(a). Adjusting the size of the leading ship does not significantly reduce its own drag, with a notable exception for the size ratio $L_0/L_1 = 2.5$. In such a case, the leading ship can receive a wave drag reduction of 25%, whereas its first follower does not achieve similar energy savings compared to other formation arrangements. As shown in Figure 8(d), a high-pressure zone emerges between the stern of the leading ship and the bow of the trailing ship, because of wave superposition. This situation is advantageous for the leading ship, which precisely rides across four waves, whereas the benefits to the first trailing ship are somewhat diminished.

When the size of the leading ship is smaller than its trailers, e.g. $L_0/L_1 = 0.5$, the leading ship receives a very small pushing force from its trailer with $C_{DR} \approx 5\%$. In such a case, the first trailing ship can receive a wave drag reduction of more than 50%, indicating that it still needs to overcome the remaining 50% of its wave drag

by generating waves. As shown in Figure 8(b), compared with other ship configurations, fewer waves are generated by the leading ships that can be harnessed by the first trailing ship.

It is also observed that the size of the leading vessel could affect the drag of the first few ships. As the trailing number increases, the drag reduction coefficient will ultimately turn to be a steady value. Figure 8(b) to (d) illustrate the wave patterns of different formations with L_0/L_1 being 0.5, 1 and 2.5, respectively. The wave patterns observed behind the first few ships in varying formations exhibit significant differences. Conversely, the wave patterns behind the last few trailing ships in any given formation tend to be similar, regardless of the size of the leading ship. It indicates that enlarging the leading vessel will exert merely a localized impact on the wave-passing amongst vessels.

For a ship with an infinite parallel section, the wave-making resistance primarily arises from its bow and stern, while the mid-body does not generate waves. Similarly, in a single-file formation, when the wave drag reduction of the trailing ships is 100%, their wave resistance is ZERO, indicating they do not generate any waves while moving on water surface. Under such case, the wave resistance of a single infinite long ship will be the same as multiple ships in a single file formation. This phenomenon is called wave-passing, as investigated by Yuan et al[14]. However, the wave drag reduction coefficient is not always 100%. It is determined by the moving speed and ship hull. As a case study shown in Figure 8(a), the wave drag reduction coefficient of each trailing ship is around 90% when a dynamic equilibrium is achieved. It indicates the trailing ships can save around 90% of the energy compared to moving independently. There is still a 10% gap to achieve "waveless". Compared with an infinite long ship these ships in a formation movement still consume more energy to maintain the waves (each one tops up 10% energy in terms of the wave).

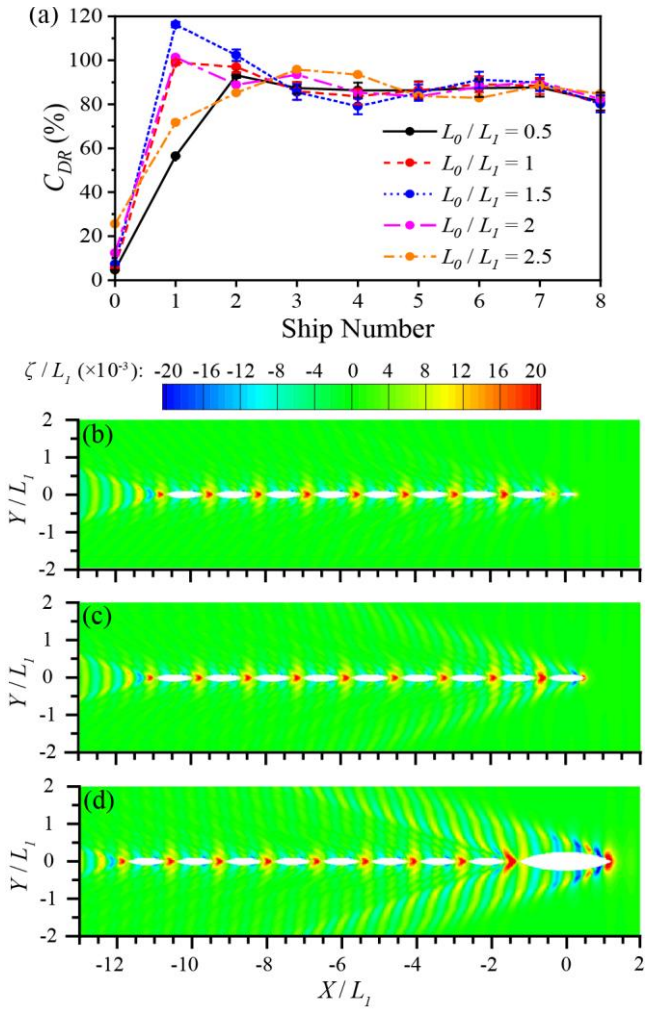

Figure8. (a) Variations in wave drag reduction for each ship across various ship formations with different sizes of the leading ship at $F_r = 0.3$. (b), (c) and (d) Wave patterns of ship formations with L_0/L_1 being 0.5, 1 and 2.5, respectively.

4.2 The sensitivity of the 1st trailing ship's position

It was found that each trailing ship could find its unique optimum position to achieve the maximum wave drag reduction. A dynamic equilibrium status was observed, where the distance between each trailing ship is the same. A question arises: what happens if one of the trailing ships does not stay in its optimum position? Here we adjust the position of the first trailing ship and calculate the drag reduction of each individual in the formation movement. The position of the first trailing ship is normalized by its own length and denoted by X_1/L_1. The results are given in Figure 9(a) when the trailing ship moves at $F_r = 0.3$, with L_0/L_1 being 1.5. At the optimal position where $X_1/L_1 = 1.6$, the first trailing ship reaps a significant reduction in drag, indicating an ideal harnessing of the leading ship's wave energy.

As the position of the first trailing ship shifts afterwards, its wave drag reduction diminishes and can even be negative, suggesting an overshoot of the optimal wave interaction zone.

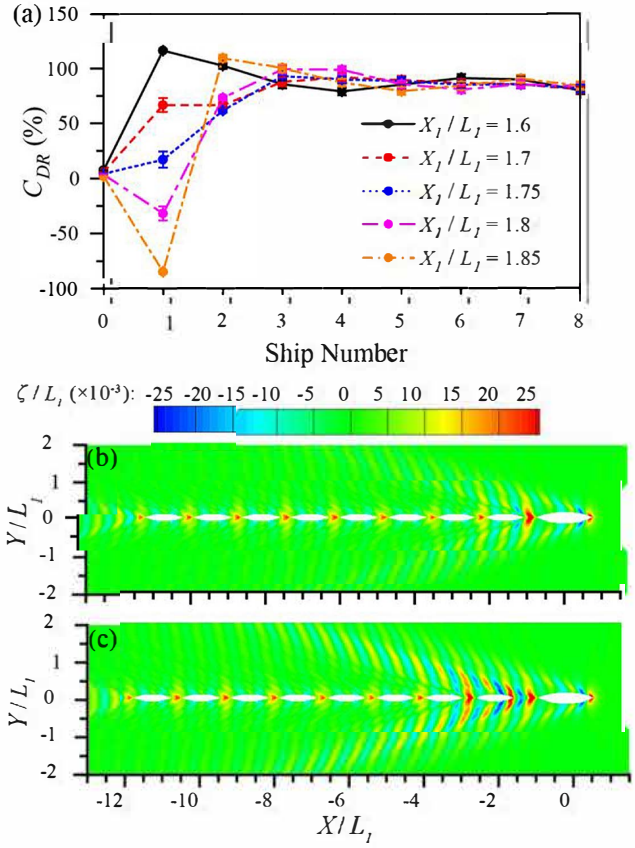

Figure 9. (a) Variations in wave drag reduction of each ship in different ship formations with changes of the first trailing ship's position at $F_r = 0.3$, and the position of the leading ship normalized by the length of the leading ship is denoted by X_1/L_1. (b) and (c) Wave patterns of ship formations with X_1/L_1 of 1.6 and 1.85, respectively.

When the first trailing ship stays at $X_1/L_1 = 1.85$, its C_{DR} drops to -84%, which is the lowest value observed across all configurations. However, this repositioning creates a wave energy profile that is highly advantageous for the second trailing ship. This ship achieves a C_{DR} of 110%, the highest amongst all configurations. This suggests that while the first trailing ship incurs a significant drag penalty for itself at this spacing, it simultaneously enhances the wave energy conditions for its follower. As shown in Figure 9(c), the constructive interference of waves between the leading ship and the first trailing ship at this specific spacing amplifies the wave energy available to the second trailing ship. The second trailing ship is positioned in such a way that it can effectively ride on the enhanced wave system, resulting in an optimal condition for drag reduction.

The wave patterns depicted in Figure 9(b) and (c) reveal that while the wave patterns of the initial ships in two separate formations differ, the patterns of the final ships within these formations are remarkably similar. This observation aligns with Figure 9(a), which demonstrates a trend of convergence in drag reduction across different formations. The proximity of the first trailing ship to the leading ship markedly influences its own drag reduction, as well as that of its immediate followers. However, this impact lessens with distance, leading the entire formation to achieve a dynamic equilibrium.

4.3 The stability of wave-passing

By decoupling the overall wave pattern into components produced individually and those generated collectively by other entities, Yuan et al.[14] explored how wave-passing can be achieved when a dedicate phase difference exists between two wave systems. To achieve a dynamic equilibrium, each trailing ship must occupy the optimum position, where the C_{DR} value reaches its maximum. As illustrated in Figure 5(a), in addition to the maximum value of C_{DR} there exist several other peak positions that can be exploited to diminish resistance. Is it possible to still achieve wave-passing when trailing ships occupy alternative peak positions? The optimum position, along with other peak positions for trailing ships within the ship formation, are selected to construct various combinations of positions. The optimum position is marked by '1', while the second and third peak positions are labelled '2' and '3', respectively.

Figure 10(a) illustrates the reduction in wave drag experienced by each vessel within various ship formations, travelling at $F_r = 0.3$. When each trailing ship occupies the optimum, second, and third peak positions, respectively denoted as '1-1-1-1-1-1-1-1', '2-2-2-2-2-2-2-2', and '3-3-3-3-3-3-3-3', the drag reduction coefficient for various formations converges to distinct values. This suggests that the wave-passing can be attained when trailing ships are positioned at peak positions other than the optimum position. As illustrated in Figure 10(d) and (e), the wave patterns behind each trailing ship can be repeated perfectly. Compared to the optimum position, the second and third peak positions shift back precisely by one and two wavelengths, respectively, with the phase differences between the two wave systems increasing by 2π and 4π, respectively. Consequently, the requisite condition for a delicate dynamic equilibrium is still satisfied. In addition, a significantly greater number of radiated waves are observed when the trailing ships occupy third peak positions, as opposed to those positioned at second peaks, which explains why the C_{DR} values of second peak positions than those of third peak positions. The C_{DR} values in these three formations converge to 88%, 60% and 53%, respectively, closely approximating the three peak values depicted in Figure 5(a). Thus, based on Figure 5(a), the converged values of C_{DR} can be inferred when the trailing vessel occupies different peak positions.

When trailing ships within the one formation occupy varying peak positions, e.g. '1-2-1-1-1-1-1' and '1-1-2-1-1-1-1', the C_{DR} values will exhibit fluctuations but will

ultimately converge to the same value as observed in '1-1-1-1-1-1-1-1-1'. The C_{DR} values at the second peak position in these two formations closely align with those in the '2-2-2-2-2-2-2-2' configuration. In both formations, as shown in Figure 10(b) and (c), the wave patterns observed behind the last few trailing ships are similar, which is also noticeably akin to the wave patterns in the '1-1-1-1-1-1-1-1-1' formation depicted in Figure 10(c).

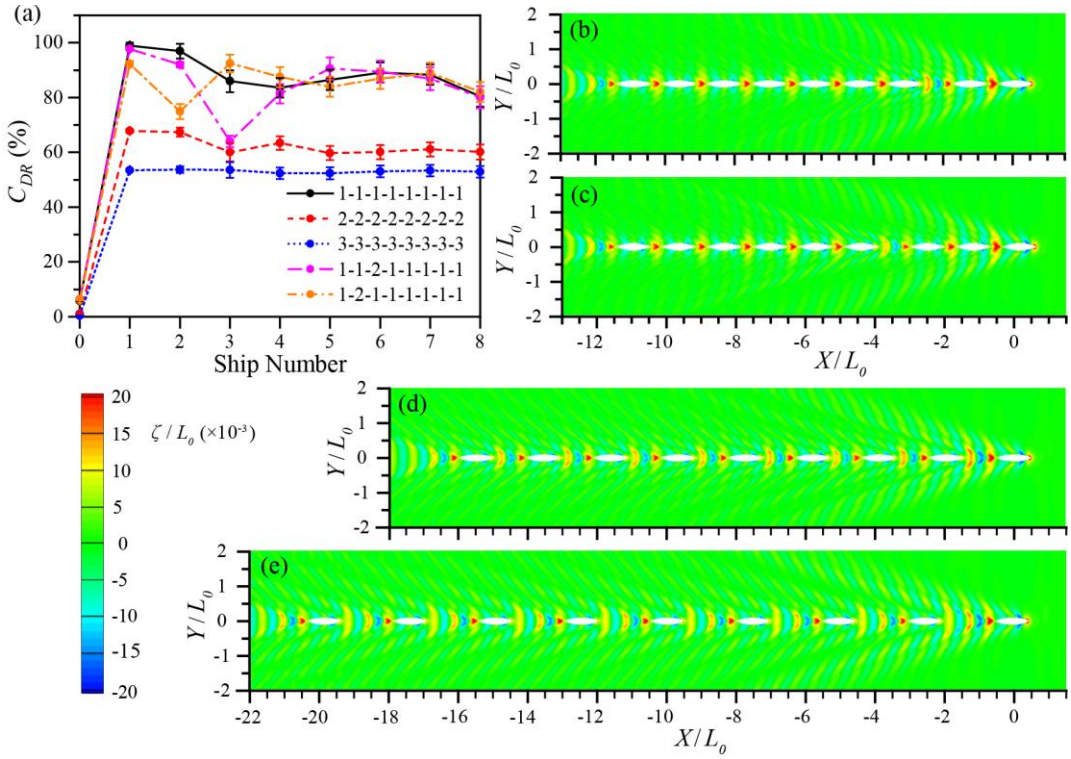

Figure10. (a) Variations in wave drag reduction of each ship at different peak positions. The optimum, second and third peak positions are denoted by 1, 2, 3, respectively. (b), (c), (d), and (e) are the Wave patterns of ship formations configured as '1-2-1-1-1-1-1-1-1', '1-1-2-1-1-1-1-1', '2-2-2-2-2-2-2-2' and '3-3-3-3-3-3-3-3', respectively.

5 Conclusions

Drawing on the discovery that ducklings use the benefits of wave-riding and wave-passing to reduce wave drag, the present study investigates the ships in a single-file configuration. To solve the steady wave interference problems, a 3D boundary element method combined with linearized free-surface boundary condition is adopted. The primary objective of this study is to explore the wave drag and wave patterns of ships arranged in different configurations. The blunt Wigley hull models are employed in numerical calculation. After numerical simulations and analyses, some of the main findings of this study are summarized as follows.

(1) The position of the trailing ship determines whether wave drag can be reduced. When positioned at a point of destructive wave interference, a win-win situation arises. The trailing vessel can utilize wave cancellation to reduce drag, while the leading vessel also experiences a slight reduction in wave drag. Conversely, at a position of constructive wave interference, the wave drag on the trailing ship increases. When the two ships are closely touched, the leading ship can gain the maximum benefit, whilst the trailing ship may have to sacrifice its own advantage.

(2) Increasing the size of the trailing vessel facilitates a reduction in the wave resistance of the leading vessel by generating a larger high-pressure zone between the two vessels. This effect of wave-riding by the leading ship is more pronounced at relatively low speed states. As speed increases, the effect of increasing the size of the trailing vessel on the wave drag reduction of the leading vessel becomes less significant.

(3) Within a formation, enlarging the leading ship has a localized effect on minimizing the drag experienced by the trailing ships. As the number of trailing ships increases, the ship formation tends to a dynamic equilibrium state.

(4) Changes in the position of individual trailing ships in a formation can have a localized effect on wave-passing. Constructive wave interference detrimentally affects the trailing ship's own drag reduction, requiring more energy to be expended to generate waves. However, this is extremely beneficial to the trailing ship immediately behind, with a more noticeable wave-riding effect.

(5) To achieve wave-passing or to reach dynamic equilibrium, each individual only needs to make sure to occupy the peak positions, which can be the second, third or any other peak position, it doesn't have to be the optimum position.

Overall, this study could provide some insight into the configuration of marine train to achieve the minimum wave resistance. It should be noted that this study mainly focuses on the wave-making resistance. Future studies are required to utilize the computational fluid dynamics (CFD) tools to calculate the total drag of ships with or without considering the propeller's wake effects.

Acknowledgements

This study was funded by the China Scholarship Council Foundation (CSC201906950057). Additionally, the numerical simulations were performed using the ARCHIE-WeSt High-Performance Computer (www.archie-west.ac.uk) based at the University of Strathclyde.

6 References

1. D. Weihs, "Hydromechanics of fish schooling," Nature **241**, 290 (1973).

2. J. C. Liao, D. N. Beal, G. V. Lauder, andM. S. Triantafyllou, "Fish exploiting vortices decrease muscle activity," Science **302**, 1566 (2003).

3. L. Li, M. Nagy, J. M. Graving, J. Bak-Coleman, G. Xie, andI. D. Couzin, "Vortex phase matching as a strategy for schooling in robots and in fish," Nature communications **11**, 5408 (2020).

4. D. Weihs, "The hydrodynamics of dolphin drafting," Journal of Biology **3**, 1 (2004).

5. R. M. May, "Flight formations in geese and other birds," Nature **282**, 778 (1979).

6. S. J. Portugal, T. Y. Hubel, J. Fritz, S. Heese, D. Trobe, B. Voelkl, S. Hailes, A. M. Wilson, andJ. R. Usherwood, "Upwash exploitation and downwash avoidance by flap phasing in ibis formation flight," Nature **505**, 399 (2014).

7. D. Hummel, "Aerodynamic aspects of formation flight in birds," Journal of theoretical biology **104**, 321 (1983).

8. C. Cutts, andJ. Speakman, "Energy savings in formation flight of pink-footed geese," Journal of experimental biology **189**, 251 (1994).

9. J.-S. Maeng, J.-H. Park, S.-M. Jang, andS.-Y. Han, "A modeling approach to energy savings of flying Canada geese using computational fluid dynamics," Journal of theoretical biology **320**, 76 (2013).

10. F. R. Hainsworth, "Precision and dynamics of positioning by Canada geese flying in formation," Journal of Experimental Biology **128**, 445 (1987).

11. M. Andersson, andJ. Wallander, "Kin selection and reciprocity in flight formation?," Behavioral Ecology **15**, 158 (2004).

12. F. E. Fish, "Energy Conservation by Formation Swimming-Metabolic Evidence From Ducklings," Mechanics and physiology of animal swimming 193 (1994).

13. F. E. Fish, "Kinematics of ducklings swimming in formation: consequences of position," Journal of Experimental Zoology **273**, 1 (1995).

14. Z.-M. Yuan, M. Chen, L. Jia, C. Ji, andA. Incecik, "Wave-riding and wave-passing by ducklings in formation swimming," Journal of Fluid Mechanics **928**, R2 (2021).

15. Z.-M. Yuan, *Wave-passing by ships in a single file formation* (Proceedings of the International Workshop on Water Waves and Floating Bodies, Giardini Naxos, Italy, 2022).

16. S. Å. Ellingsen, "Getting the ducks in a row," Journal of Fluid Mechanics **932**, F1 (2022).

17. M. Wilson, C. Hsu, andD. Jenkins, *Experiments and predictions of the resistance characteristics of a wave cancellation multihull ship concept* (SNAME, 1992).

18. E. O. Tuck, andL. Lazauskas, "Optimum hull spacing of a family of multihulls," Ship Technology Research-Schiffstechnik **45**, 180 (1998).

19. H. Peng, "Numerical computation of multi-hull ship resistance and motion," (2001).

20. D. Yu, P. Lecointre, andR. W. Yeung, "Experimentally-based investigation of effects of wave interference on the wave resistance of asymmetric di-hulls," Applied Ocean Research **65**, 142 (2017).

21. B. Yildiz, B. Soner, S. Duman, andR. Datla, "A numerical and experimental study on the outrigger positioning of a trimaran hull in terms of resistance," Ocean Engineering **198**, 106938 (2020).

22. R. Deng, C. Li, D. Huang, andG. Zhou, "The effect of trimming and sinkage on the trimaran resistance calculation," Procedia Engineering **126**, 327 (2015).

23. A. Nazemian, andP. Ghadimi, "CFD-based optimization of a displacement trimaran hull for improving its calm water and wavy condition resistance," Applied Ocean Research **113**, 102729 (2021).

24. C. Ma, X. Zhao, X. Cheng, Y. Yang, andL. Fan, "The wave interference and the wave drag of a leader–follower ship fleet," Ocean Engineering **274**, 114089 (2023).

25. Z. Liu, C. Dai, X. Cui, Y. Wang, H. Liu, andB. Zhou, "Hydrodynamic Interactions between Ships in a Fleet," Journal of Marine Science and Engineering **12**, 56 (2023).

26. Y. He, J. Mou, L. Chen, Q. Zeng, Y. Huang, P. Chen, andS. Zhang, "Will sailing in formation reduce energy consumption? Numerical prediction of resistance for ships in different formation configurations," Applied Energy **312**, 118695 (2022).

27. Z. Dong, X. Liang, X. Guan, andW. Li, "Formation optimization of various spacing configurations for a fleet of unmanned surface vehicles based on a hydrodynamic energy-saving strategy," Ocean Engineering **266**, 112824 (2022).

28. Z. Dong, X. Liang, D. Liu, C. Yu, andW. Li, "Dynamic formation optimisation for energy saving of a fleet of unmanned surface vehicles based on robust optimisation over time strategy," Ocean Engineering **301**, 117382 (2024).

29. W. B. Lambert, andS. Brizzolara, *Wave Resistance Reduction for Ships Traveling in Fleet Formation* (SNAME, 2020).

30. Y. Qin, C. Yao, Y. Zheng, andJ. Huang, *Study on Hydrodynamic Performance of a Conceptional Sea-Train* (American Society of Mechanical Engineers, 2022).

31. DARPA, Sea train Document No. Number, 2020.

32. H. Lackenby, "The thirty-fourth Thomas Lowe gray lecture: resistance of ships, with special reference to skin friction and hull surface condition," Proceedings of the Institution of Mechanical Engineers **176**, 981 (1962).

33. Z.-M. Yuan, P. Kellet, A. Incecik, O. Turan, andE. Boulougouris, "Ship-to-ship interaction during overtaking operation in shallow water," Journal of Ship Research **59**, 172 (2015).

34. J. M. Journee, "Experiments and calculations on four Wigley hullforms," TUDelft, Faculty of Marine Technology, Ship Hydromechanics Laboratory, Report No. 909 (1992).

35. Y. Kim, D. K. Yue, andB. S. Connell, "Numerical dispersion and damping on steady waves with forward speed," Applied Ocean Research **27**, 107 (2005).